Evaluation of macrocyclic hydroxyisophthalamide ligands as chelators for zirconium-89

Nikunj B. Bhatt[1�é], **Darpan N. Pandya**[1�é], **Jide Xu**[2], **David Tatum**[2], **Darren Magda**[2]*, **Thaddeus J. Wadas**[1]*

1 Department of Cancer Biology, Wake Forest School of Medicine, Winston-Salem, North Carolina, United States of America, **2** Lumiphore, Inc., Berkeley, California, United States of America

�é These authors contributed equally to this work.
* twadas@wakehealth.edu (TJW); dmagda@lumiphore.com (DM)

Abstract

The development of bifunctional chelators (BFCs) for zirconium-89 immuno-PET applications is an area of active research. Herein we report the synthesis and evaluation of octadentate hydroxyisophthalamide ligands (**1** and **2**) as zirconium-89 chelators. While both radiometal complexes could be prepared quantitatively and with excellent specific activity, preparation of ^{89}Zr-**1** required elevated temperature and an increased reaction time. ^{89}Zr-**1** was more stable than ^{89}Zr-**2** when challenged *in vitro* by excess DTPA or serum proteins and *in vivo* during acute biodistribution studies. Differences in radiometal complex stability arise from structural changes between the two ligand systems, and suggest further ligand optimization is necessary to enhance ^{89}Zr chelation.

Introduction

The development of zirconium-89 (^{89}Zr: $t_{1/2}$ = 78.4 h; β^+; 23%, 909 keV)-based PET radiopharmaceuticals has intensified since comprehensive procedures for producing ^{89}Zr in high specific activity and attaching it to monoclonal antibodies (mAbs) were first described [1–3]. The half-life and positron emission properties of ^{89}Zr make it ideal for the labeling of mAbs, which require extended circulation time for effective *in vivo* antigen targeting. Several ^{89}Zr-labeled mAbs are currently in clinical trials [4–6].

The most widely used bifunctional chelators (BFCs) for ^{89}Zr chelation are desferrioxamine (DFO) and its analogues, which are derivatives of the iron chelator desferral, a siderophore secreted by *Streptomyces pilosus* [7,8]. Although DFO contains three hydroxamate groups, which seem to provide effective chelation for ^{89}Zr *in vitro*, this leaves 2 empty coordination sites for the 8-coordinate ^{89}Zr and published reports described elevated bone retention in murine models receiving injections of ^{89}Zr-DFO-labeled agents [9,10]. Several papers have attempted to explain this phenomenon through molecular modeling and experimental studies [11,12]. Further investigations have attempted to enhance the stability of the ^{89}Zr-DFO complex or design new ligands as BFCs for ^{89}Zr [13–24].

In this report, we describe the development of BFCs containing four 2-hydroxyisophthalamide coordinating units for ^{89}Zr chelation (Fig 1). We became interested in hydroxyisophthalamide (IAM) based-ligands, since these coordination motifs are similar to those used by bacteria for metal ion sequestration and have been used successfully as chelators for a variety of lanthanide metal cations [25–32]. Additionally, they offer potential advantages for ^{89}Zr BFC design [33]. These aromatic systems bind through a combination of phenolic and carbonyl oxygen atoms, which should aid coordination to hard radiometals such as zirconium. Furthermore, the IAM unit can be easily derivatized to quickly expand the diversity of ligands that can be synthesized and evaluated.

Materials and methods

Zirconium-89 (^{89}Zr: $t_{1/2}$ = 78.4 h, β^+: 22.8%, $E_{\beta+max}$ = 901 keV; EC: 77%, E_γ = 909 keV) was purchased from Washington University School of Medicine (St. Louis, MO) or Zevacor, Inc. (Dulles, VA). Unless otherwise noted, all other chemicals were purchased from Sigma-Aldrich Chemical Co. (St. Louis, MO), and solutions were prepared using ultrapure water (18 MΩ-cm resistivity). Radiochemistry reaction progress and purity were analyzed using a Waters analytical HPLC (Milford, MA), which runs Empower software and is configured with a 1525 binary pump, 2707 autosampler, 2998 photodiode array detector, 2475 multi-channel fluorescence detector, 1500 column heater, fraction collector, Grace Vydac 218MS C18 column (5 μm, 4.6 × 250 mm, Grace Davidson, DeerField, IL) and a Carrol Ramsey 105-s radioactivity detector (Berkeley, CA). All ligands (**1** and **2**) and associated ^{Nat}Zr-complexes were monitored at 220 nm using a mobile phase consisting of 0.01% TFA/H$_2$O (solvent A) and 0.01% TFA/acetonitrile (solvent B), and a gradient consisting of 0% B to 70% B in 20 min at a flow rate of 1.2 mL/min. In addition, radio-TLC was conducted on a Bioscan AR 2000 radio-TLC scanner equipped with a 10% methane:argon gas supply and a PC interface running Winscan v.3 analysis software (Eckert & Ziegler, Berlin, DE). Varian ITLC-SG strips were employed using a 50 mM DTPA (pH 7) solution as eluent, and the complex ^{89}Zr(ox)$_2$ as a standard control. Radioactive samples were counted using a Perkin Elmer 2480 Wizard$^®$ gamma counter (Waltham, MA). Preparation of ligand **1** has been reported [27]. Starting compound **3**, which was used for the synthesis of **2**, was synthesized as described previously [32].
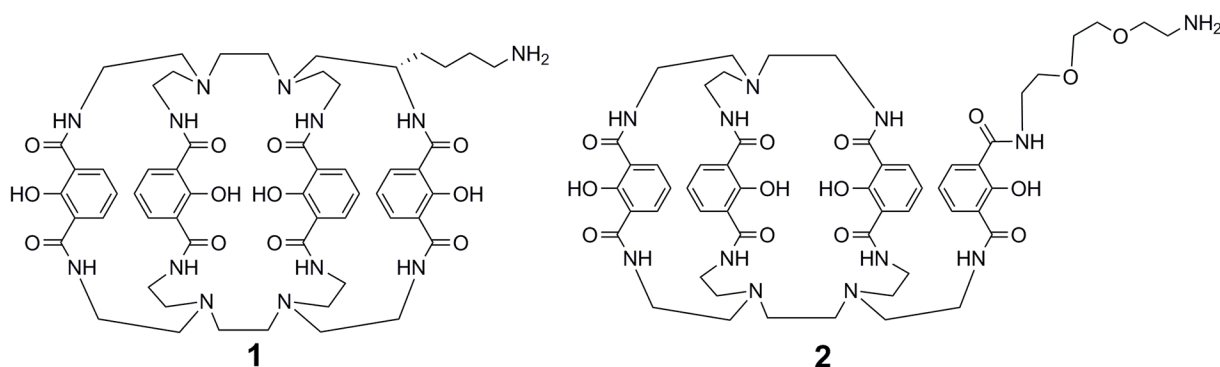
Fig 1. BFCs 1 and 2. These ligands contain 2-hydroxyisophthalamide units for octadentate coordination of Zr^{4+} and a pendant arm containing a primary amine, which can be easily functionalized for conjugation to a variety of targeting ligands.

https://doi.org/10.1371/journal.pone.0178767.g001

Synthesis

N,N',N'',N'''-[1,2-ethanediylbis(nitrilodi-2,1-ethanediyl)]tetrakis{2-benzyloxy-3-[(2-thioxo-3-thiazolidinyl)carbonyl]benzamide} (5). Tetrakis-(2-aminoethyl) ethylene diamine **4** (581 mg, 2.50 mmol) was dissolved in ca. 10% isopropyl alcohol in dichloromethane (48 mL) and triethylamine (1.74 mL, 12.5 mmol) and added using a syringe pump (NE1000) to a solution of 2-benzyloxy-1,3-phenylenebis((2-thioxothiazolidin-3-yl)methanone) **3** (23.7 g, 50 mmol) in dichloromethane (anhydrous, 100 mL) and triethylamine (1.74 mL, 12.5 mmol) over 50 h at a rate of 1.00 mL/hr. After a further 24 h, solvent was removed under reduced pressure, and the crude product was purified by silica gel chromatography using 0.1% triethylamine, 2–5% isopropyl alcohol in dichloromethane as eluents. Fractions containing product were combined, solvent was removed under reduced pressure, and the residue dried *in vacuo* to provide compound **5** (1.611 g, 39.0%). ^{1}H NMR (300 MHz, CDCl$_3$): δ = 8.02–7.99 (d of d, 4H, ArH), 7.46–7.44 (m, 8H, ArH), 7.30–7.20 (m, 20H, PhH), 4.96 (s, 8H, PhCH$_2$O), 4.39 (t, 8H, NCH$_2$CH$_2$S), 3.26 (m, 8H, CH$_2$NC = O), 3.02 (t, 8H, NCH$_2$CH$_2$S), 2.38 (m, 12H, CH$_2$N). ^{13}C NMR (300 MHz, CDCl$_3$): δ = 201, 167, 165, 154, 136, 134, 132, 130, 129, 128, 125, 59, 55, 53, 52, 38, 29. FTMS pESI: calculated for C$_{82}$H$_{81}$N$_{10}$O$_{12}$S$_8$ [MH]$^+$, 1653.3796, found, 1653.3855.

Benzyl-protected bi-macrocycle (7). A solution of tris-(2-aminoethyl)amine **6** (54 mg, 365 μmol) in isopropyl alcohol (50 mL) and triethylamine (255 μL) and a solution of N,N',N'', N'''-[1,2-ethanediylbis(nitrilodi-2,1-ethanediyl)]tetrakis[2-benzyloxy-3-[(2-thioxo-3-thiazolidinyl) carbonyl]benzamide **5** (213 mg, 528 μmol) in dichloromethane (50 mL) were added dropwise to a solution of dichloromethane (1.50 L) and triethylamine (255 μL), degassed three times with N$_2$, over 4 days using two syringe pumps at 0.5 mL/hr. After an additional day of reaction, solvent was removed under reduced pressure, and the crude product was purified by silica gel chromatography using 0.1% triethylamine, 2–7.5% isopropyl alcohol in dichloromethane as eluents. Fractions containing product were combined, solvent was removed under reduced pressure, and the residue dried *in vacuo* to provide the protected bi-macrocycle **7** (167 mg, 31.7%). ^{1}H NMR (300 MHz, CDCl$_3$): δ = 7.94–6.74 (broad m, 32H, PhH, ArH), 5.00 (s, 2H, PhCH$_2$O), 4.80–4.75 (br s, 6H, PhCH$_2$O), 4.48 (t, 2H, NCH$_2$CH$_2$S), 3.50–3.32 (m, 14H, CH$_2$NC = O), 3.17 (t, 2H, NCH$_2$CH$_2$S), 2.64–2.26 (m, 18H, CH$_2$N). ^{13}C NMR (600 MHz, CDCl$_3$): δ = 201.6, 167.3, 167.0, 166.6, 166.3, 165.5, 164.7, 154.5,153.3, 153.2, 136.0, 135.1, 134.1, 133.2, 132.7, 131.7, 130.3, 129.4, 129.2, 129.1, 128.8, 128.6, 128.4, 127.7, 127.5, 124.6, 124.4, 79.0, 78.4, 77.7, 72.5, 71.6, 71.2, 70.4, 70.1, 61.8, 55.7, 55.3, 55.0, 54.2, 52.9, 52.4, 51.9, 51.2, 50.2, 48.8, 39.1, 38.3, 37.8, 37.5, 31.6, 29.6, 28.7, 26.6, 19.2, 13.9. FTMS pESI: calculated for C$_{79}$H$_{84}$N$_{11}$O$_{12}$S$_2$ [M+H]$^+$, 1442.5737, found, 1442.5753.

Benzyl and *tert*-butyloxycarbonyl-protected bi-macrocycle (9). A solution of benzyl-protected bi-macrocycle **7** (154 mg, 108 μmol) in dry dichloromethane (5 mL) and triethylamine (74 μL) was treated with N-Boc-2,2'-(ethylenedioxy)diethylamine **8** (40 mg, 161 μmol) under N$_2$, and stirred for 28 h. Solvent was removed under reduced pressure, and the crude product was purified by silica gel chromatography using 0.1% triethylamine, 3.5–5% methanol in dichloromethane as eluents. Fractions containing product were combined, solvent was removed under reduced pressure, and the residue dried *in vacuo* to provide the protected bi-macrocycle **9** (148 mg, 87%). ^{1}H NMR (300 MHz, MeOD): δ = 7.8–6.9 (broad m, 32H, PhH, ArH), 5.5 (s, 2H, PhCH$_2$O), 3.6–3.1 (m, 26H, CH$_2$CH$_2$O, CH$_2$NC = O), 2.7–2.4 (m, 18H, CH$_2$N), 1.4 (s, 9H, CH$_3$). ^{13}C NMR (300 MHz, MeOD): δ = 154.4, 153.7, 136.5, 132.5, 132.0, 129.4, 129.0, 128.6, 124.7, 124.5, 79.2, 78.5, 78.1, 70.2, 69.2, 53.9, 50.0, 40.2, 39.8, 39.1, 38.3, 38.0, 27.8. FTMS pESI: calculated for C$_{87}$H$_{103}$N$_{12}$O$_{16}$ [M+H]$^+$, 1571.7610, found, 1571.7667.

Bi-macrocyclic bifunctional chelator (2). Benzyl and *tert*-butyloxycarbonyl-protected bi-macrocycle **9** (89 mg, 57 μmol) was dissolved in 12N hydrochloric acid (1.5 mL) and glacial acetic acid (1.5 mL). The solution was stirred under an inert atmosphere for 26 h, whereupon HCl was removed with a stream of inert gas. Solvents were removed under reduced pressure and the residue was dried *in vacuo*. The residue was dissolved in methanol (2000 μL) and transferred to four O-ring microcentrifuge tubes. Ether (ca. 1.5 mL) was added, and the tubes were placed at 4°C for 1 h. The tubes were centrifuged at 12,000 rpm for 3 min and decanted. Pellets were washed with ether (ca. 1.5 mL), allowed to air dry, and then dried *in vacuo* to provide bi-macrocycle **2**, tetrahydrochloride salt (58.6 mg, 82%). ^{1}H NMR (500 MHz, CD$_3$OD, 25°C): δ 8.18–7.43 (m, 8H), 7.05–6.48 (m, 4H), 4.36–3.23 (m, 42H), 2.97 (s, 2H). ^{13}C NMR (100 MHz, CDCl3, 25°C): δ 120.11, 71.52, 71.49, 70.50, 40.80, 40.56 (note: broad signals due to macrocyclic structure impeded full characterization of the ^{13}C resonances). FTMS pESI: calculated for C$_{54}$H$_{71}$N$_{12}$O$_{14}$ [M+H]$^+$, 1111.5207, found, 1111.5234. Anal: Calculated (found) C$_{54}$H$_{84}$N$_{12}$O$_{19}$Cl$_4$, 48.13 (48.15), 6.29 (6.22), 12.48 (12.11).

Zr-1. Compound **1** (6.9 mg, 5.1 mmol) was dissolved into methanol (200 μL), and Zr (acac)$_4$ (1.94 mg, 3.98 mmol) was separately dissolved into methanol (200 μL). The solutions were combined and allowed to sit at room temperature for 1 hour. Triethylamine (1.5 mL) was added, causing a white precipitate to form. The precipitate was isolated by centrifugation, and the supernatant was removed. The solid residue was then dissolved into methanol (400 μL) and again precipitated by adding triethylamine (1.5 mL). The product was dissolved and precipitated in this way a total of 3 times, and then the residual solvent was removed under vacuum, yielding a white solid of Zr-**1**. Yield: 3.78 mg, 66%. ^{1}H NMR (500 MHz, CD$_3$OD, 25°C): δ 7.81–7.23 (m, 8H), 6.54–6.08 (m, 4H), 3.42–3.12 (m, 42H), 2.77 (s, 2H). HRMS-ESI (*m/z*, [M+H]$^+$) Calcd for C$_{56}$H$_{70}$N$_{13}$O$_{12}$^{90}Zr: 1206.4308, Found: 1206.4348. Anal. Calcd (Found) for ZrC$_{56}$H$_{69}$N$_{13}$O$_{12}$·1.5C$_6$H$_{16}$NCl·1.5H$_2$O: C 54.18 (54.22), H 6.72 (6.69), N 14.09 (14.06) %.

Zr-2. Compound **2** (5.5 mg, 4.1 mmol) was dissolved into methanol (200 μL), and Zr (acac)$_4$ (1.44 mg, 2.95 mmol) was separately dissolved into methanol (200 μL). The solutions were combined and allowed to sit at room temperature for 1 hour. Triethylamine (1.5 mL) was added, causing a white precipitate to form. The precipitate was isolated by centrifugation, and the supernatant was removed. The solid residue was then dissolved into methanol (400 μL) and again precipitated by adding triethylamine (1.5 mL). The product was dissolved and precipitated in this way a total of 3 times, and then the residual solvent was removed under vacuum, yielding a white solid of Zr-**2**. Yield: 2.83 mg, 71%. ^{1}H NMR (500 MHz, CD$_3$OD, 25°C): δ 7.91–7.43 (m, 8H), 6.48–6.02 (m, 4H), 3.62–3.12 (m, 42H), 2.85 (s, 2H). HRMS-ESI (*m/z*, [M+H]$^+$) Calcd for C$_{54}$H$_{67}$N$_{12}$O$_{14}$^{90}Zr: 1197.3947, Found: 1197.4004. Anal. Calcd (Found) for ZrC$_{54}$H$_{66}$N$_{12}$O$_{14}$·2C$_6$H$_{16}$NCl·H$_2$O: C 53.14 (53.24), H 6.76 (6.67), N 13.15 (13.03) %.

Density functional theory calculations

Ground state density functional theory calculations were performed at the Molecular Graphics and Computational Facility, College of Chemistry, University of California, Berkeley using Gaussian 09 [34]. The ground state geometries of Zr-**1** and Zr-**2** (S3 Fig and S1 Table) were optimized using the B3LYP functional, treating the light atoms (H through O) with the 6-31G (d,p) basis set [35–38]. The Zr atom was treated with the effective core potential MWB28 [39,40]. No solvent, symmetry constraints, or counterions were included in the calculations. Crystal structures of the related H22 linked 2-hydroxyisophthalamide (IAM) ligands bound to Tb^{III} were used as starting points for these Zr^{IV} complexes [27]. In addition to geometry optimizations, frequency calculations were performed, and all structures are presented in energy minimized conformations.

Radiolabeling of macrocyclic 2-hydroxyisophthalamide ligands (1, 2) with ^{89}Zr

The complexation of ^{89}Zr with macrocyclic 2-hydroxyisophthalamide ligands (**1**, **2**) was achieved by reacting 5–10 μg (5–10 μL,1.0 mg/mL in water) of each ligand with an aliquot of ^{89}Zr(ox)$_2$ (0.6 mCi, 22.2 MBq) diluted in 100 μL of water and pH adjusted to 7–7.5 using 1 M Na$_2$CO$_3$. The ^{89}Zr-**1** reaction was incubated at 95˚C for 2 h; the ^{89}Zr-**2** reaction was incubated at 50˚C for 1 h. Formation of ^{89}Zr-**1** and ^{89}Zr-**2** was monitored by radio-TLC using Varian ITLC-SG strips and 50 mM DTPA (pH 7) as the mobile phase. In this system, unchelated ^{89}Zr forms a complex with DTPA and elutes near the solvent front (denoted as the red line at 130 mm in radio-TLC chromatograms); the ^{89}Zr-ligand complex remains at the origin (denoted as the red line at 30 mm in radio-TLC chromatograms) (S4 Fig). The identity of each radioactive complex was further confirmed by comparing its radio-HPLC elution profile to the UV-HPLC spectrum of its nonradioactive Zr-complex (S5 and S6 Figs).

Determination of partition coefficients (log P)

The partition coefficient (log P) for each complex was determined by adding 5 μL of each ^{89}Zr-labeled complex (5 μCi; 0.19 MBq) to a mixture of 500 μL of octanol and 500 μL of water [41]. The resulting solutions (n = 8) were vigorously vortexed for 5 min at room temperature and then centrifuged for 5 min to ensure complete layer separation. From each sample, a 50 μL aliquot was removed from each phase. Radioactivity in each phase was counted separately in a gamma counter. Each organic phase was washed with water before gamma counting. The partition coefficient was calculated as a ratio of counts in the octanol fraction to counts in the water fraction. The log P values were reported as an average of four measurements (S2 Table).

In vitro serum stability and DTPA challenge study

In vitro stability was carried out by adding 10 μL of each ^{89}Zr-labeled complex (50 μCi, 1.85 MBq) to 500 μL DTPA (50 mM, pH7), or human serum (S3 Table). The solutions (n = 3) were incubated at room temperature and 37˚C, respectively. Samples were analyzed daily for 7 days using radio-TLC (Varian ITLC-SG strips and 50 mM DTPA (pH 7)) and gamma counting (energy window: 500–1500 keV) [9].

Animal model

All studies were carried out in strict accordance with the recommendations in the Guide for the Care and Use of Animals of the National Institutes of Health, and approved by the Wake Forest University Health Sciences Institutional Animal Care and Use Committee (Protocol # A14-081). Normal mice used in the experiments were received from The Jackson Laboratory, USA and were accommodated in the housing room operated according to the Animal Welfare Act, the guidelines established by the NIH and all other Federal and State statutes and regulations pertaining to laboratory animal care. All animals were acclimated to a 12-hour light/dark cycle and received food and water *ad libitum*. All animals were checked by veterinary staff daily to ensure well-being, proper environment and monitor for signs of distress. Clinical signs of distress in laboratory rodents include decreased activity, pilo-erection, un-groomed appearance, excessive licking and scratching, self-mutilation, abnormal stance, hunched appearance, rapid or shallow respiration, grunting, dilated pupils, aggressiveness towards handler, high pitch vocalizations, change in feeding activity, and attempts to separate from group. In the event of clinical distress, animals were euthanized after consulting the on-call veterinarian. To minimize suffering during the tail vain injection, animals were kept under deep

isoflurane anesthesia. At the end point of the study, animals were anesthetized with isoflurane and were euthanized by cervical dislocation, which is consistent with the recommendations of the American Veterinary Medical Association guidelines on Euthanasia. Animals were monitored every 30 minutes during the experiment, but during the experiment, none of the animals died or were found ill before experimental end point.

Biodistribution studies

Biodistribution studies were based upon a previously published procedure [42]. Briefly, female NIH Swiss mice (6–8 wk old, n = 6) were injected with each ^{89}Zr-labeled complex (0.55 MBq (15 μCi)/mouse) via the tail vein, and sacrificed at 2, 4, 24, 48 and 72 h post-injection. Organs and tissues of interest were excised and weighed, and radioactivity was counted on a gamma counter. The percent injected dose per gram (%ID/g) was calculated by comparison to a weighed, counted standard for each group (S5 and S6 Tables).

Statistical methods

All of the data are presented as mean±SD or mean (95% confidence intervals). For statistical classification a Student's t test (two-tailed, unpaired) or one-way anova (with Tukey's multiple comparison post-test) was performed using GraphPad Prism software (San Diego, CA). $p < 0.05$ was considered significant.

Results and discussion

Ligand **1** was synthesized according to published procedures [27]. Preparation of an IAM bi-macrocyclic ligand **2** (Scheme 1) began with 2-benzyloxy-1,3-phenylenebis((2-thioxothiazolidin-3-yl)methanone) **3**, which was condensed with tetrakis-(2-aminoethyl) ethylene diamine **4** under pseudo-first order conditions to provide the activated tetra-amide **5**. This was reacted with tris-(2-aminoethyl)amine **6** under high dilution conditions to form the bi-macrocycle **7**. The remaining activated amide in **7** was reacted with amine **8** to provide bi-macrocycle **9**. Protective groups were removed using a solution of concentrated hydrochloric acid in acetic acid to provide bi-macrocycle **2**. Both ligand **1** and ligand **2** were completely characterized and observed using NMR spectroscopy, high resolution mass spectrometry and elemental analysis. The nonradioactive Zr-**1** and Zr-**2** complexes were prepared by reacting ligands (**1** and **2**, 1 equiv. each) with Zr(acac)$_4$ (0.75 equiv.) in methanol. Characterization of both complexes by NMR revealed spectra containing a complex pattern of multiplets that could not be resolved further. However, high resolution mass spectrometry (S1 and S2 Figs) and elemental analysis confirm the identity of each complex. Interestingly, several peaks were observed in the UV-HPLC chromatograms (S5 and S6 Figs), but based upon mass spectrometry and elemental analysis, it is believed that these peaks are structural isomers that form upon the coordination of the Zr^{4+} ion in solution. It is not implausible to imagine the formation of several structural isomers, which are dependent upon the number of phenolic and carbonyl oxygen atoms involved in metal ion complexation. Attempts were made to isolate each isomer by HPLC for NMR analysis, but isomeric inter-conversion was observed during this process, which made our attempts at further characterization unsuccessful. While attempts to elucidate the molecular structure of Zr-IAM complexes using single crystal x-ray diffraction analysis are ongoing, we performed density functional theory calculations on both Zr-**1** and Zr-**2** to model ground state coordination geometries (S1 Table). If we neglect the alkyl amine linker arm, the structure of Zr-**1** (S3 Fig) has twofold rotational symmetry, where the symmetry axis passes through the midpoint of the central ethylene units and through the metal center. Modeling revealed the energy minimized structure of Zr-**2** could exist with two distinct binding modes (A or B;

S3 Fig), although both are quite similar. In structure A, the amine sidearm is connected to the amide not involved in Zr^{4+} ion coordination. In structure B, the amine sidearm is connected to the amide directly involved in Zr^{4+} ion coordination. Despite these differences, structure A was found to be only 0.42 kcal/mol lower in energy than structure B, which is a very small difference given the size and flexibility of the ligands. Thus it is likely that both A and B are present at significant quantities in solution, which further suggests that the multiple peaks observed in the HPLC chromatograms result from coordination isomers in solution.

**Scheme 1**. **Synthesis of bi-macrocyclic bifunctional chelator 2.**

Scheme 2. **Radiochemical synthesis of [89]Zr-1 and [89]Zr-2.** Proposed structures of [89]Zr-1 and [89]Zr-2 are depicted, but other structural isomers may be possible.

Our initial radiochemistry studies with **1** revealed that elevated reaction time and temperature were necessary for quantitative radiolabeling (S4 Fig). Although quantitative radiolabeling was achieved, these conditions would be too harsh for radiolabeling of **1**-mAb conjugates. Accordingly, we reduced the structural rigidity of **1** by partially uncoupling one of the iso-phthalamide coordinating units to yield **2**. Using this strategy, the time and temperature needed to quantitatively radiolabel **2** with [89]Zr (S4 Fig) decreased markedly. Furthermore, an A_s of 0.7 GBq/μmol was observed, which is comparable to the A_s of similar [89]Zr-complexes reported in the literature [14,19,23].

Lipophilicity (log P) plays an essential role in estimating the biodistribution of [89]Zr-complexes *in vivo* [41]. Using the water-octanol partition method, the log P (pH 7) of [89]Zr-**1** and [89]Zr-**2** was determined to be -2.97±0.02 and -1.45±0.06, respectively, compared to -2.83±0.04 for [89]Zr-**DFO** (S2 Table). These negative values suggest that the complexes possess hydrophilic character, which is expected to result from the abundant hydrogen bonding motifs displayed by the radiometal complexes while in solution. These values are similar to recently published values for [89]Zr-terepthalamide and [89]Zr-hydroxypyridinone complexes [14,19,23]. Complexes of **1** and **2** also contain 4 and 3 tertiary amines in the scaffold, respectively, in addition to the primary amines, some of which might be protonated at neutral pH.

Initial stability studies were also conducted by incubating [89]Zr-**1** or [89]Zr-**2** in the presence of a 50 mM DTPA solution over 7 days (S3 Table). [89]Zr-**1** was more resistant to DTPA challenge than [89]Zr-**2**. Only 15% and 28% of [89]Zr-**1** underwent transchelation after 1 and 7 days, respectively, while 37% and 74% of [89]Zr-**2** underwent transchelation during the same study period. [89]Zr-**DFO** displayed stability similar to [89]Zr-**2** under these conditions, with 45% and 59% transchelation after 1 and 7 days, respectively. Likewise, incubation in human serum revealed [89]Zr-**1** was more resistant to serum protein challenge than [89]Zr-**2** (S4 Table). While 75% of [89]Zr-**1** remained intact after 7 days, only 17% of [89]Zr-**2** was observed at the same time point. [89]Zr-**DFO** remained intact upon incubation with serum. The resistance of [89]Zr-**1** vs. [89]Zr-**DFO** to DTPA challenge may arise from the enhanced binding that occurs through the four IAM units, which can accommodate the [89]Zr^{4+} ion to form an eight coordinate complex. On the other hand, reduced stability of [89]Zr-**2**, observed as [89]Zr^{4+} ion transchelation to DTPA or serum proteins, may be caused by the reduced structural rigidity of ligand **2**, which results in dissociation of an IAM coordinating unit and subsequent loss of the coordinated [89]Zr^{4+} ion.

[89]Zr-**1** and [89]Zr-**2** were evaluated *in vivo* through biodistribution studies in normal mice. Fig 2 displays the clearance properties of [89]Zr-**1**, [89]Zr-**2** and [89]Zr-**DFO** from the blood, liver, kidney, and bone; and complete biodistribution details can be found in SI (S5–S7 Tables). Animals injected with [89]Zr-**1** and [89]Zr-**2** demonstrated elevated levels of radioactivity in the blood at early time points when compared to animals injected with [89]Zr-**DFO** [19]. However by 72 h p.i., blood retention was comparable in animals receiving [89]Zr-**DFO** and [89]Zr-**1**, but not [89]Zr-**2**. ([89]Zr-**DFO** vs. [89]Zr-**1** vs. [89]Zr-**2**: (mean%ID/g±SD; [one-way ANOVA]: 0.00033±0.0008 vs.
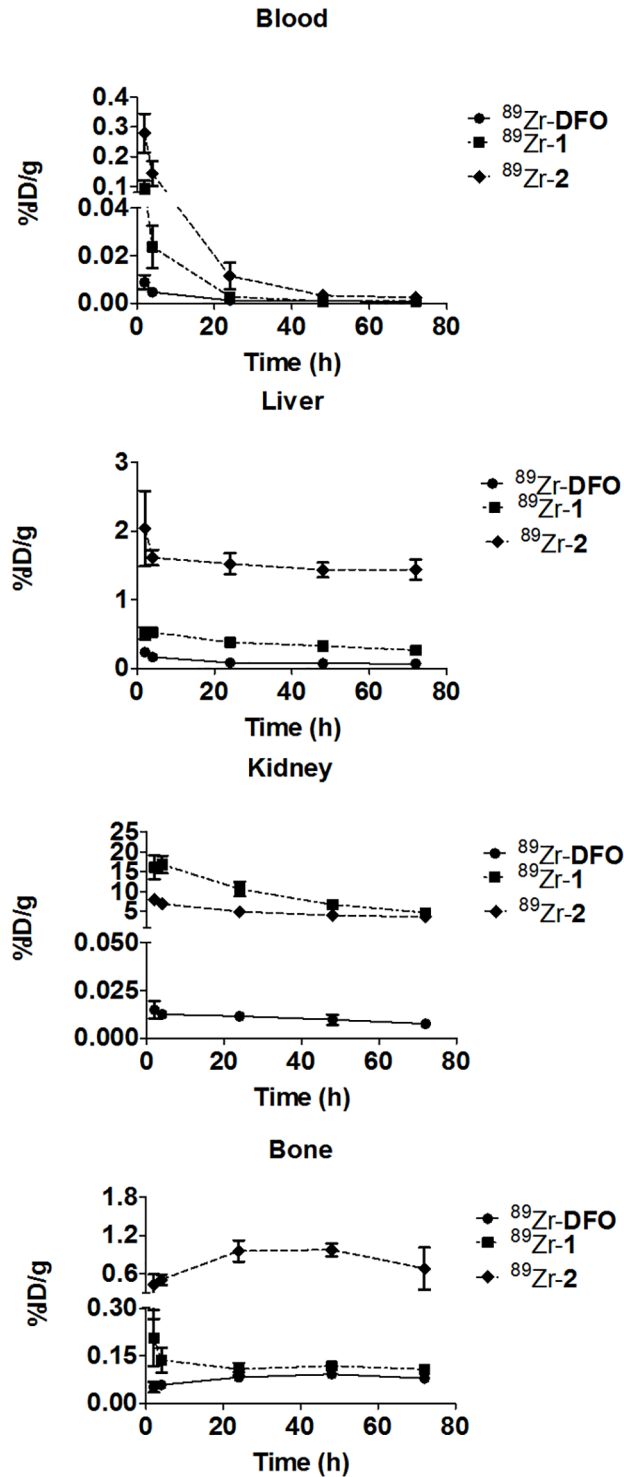
Fig 2. Biodistribution and clearance of [89]Zr-DFO, [89]Zr-1, and [89]Zr-2 from selected tissues. [89]Zr-DFO demonstrated a more favorable biodistribution than [89]Zr-1 and [89]Zr-2. [89]Zr-DFO data is taken from reference 19.

https://doi.org/10.1371/journal.pone.0178767.g002

0.0008±0.0008 vs. 0.002±0.001; [F(2,15) = 40.23, p < 0.0001]). These differences, especially at earlier time points, may relate to the different ligand systems used to chelate ^{89}Zr.

DFO is a hexadentate acyclic ligand that forms a +1 charged complex. Conversely, **1** is a tri-macrocycle comprised of 24 and 30-atom rings, whereas **2** forms a bi-macrocyclic complex of 24 and 27 membered rings; both ligands are octadentate (Fig 1). The altered charge of ^{89}Zr-**1** and ^{89}Zr-**2** when compared to ^{89}Zr-**DFO** might enhance their interactions with serum proteins, which retard clearance from the blood stream. These observations correlate well with the *in vitro* serum stability data obtained for both ^{89}Zr-IAM complexes.

By 72 h p.i., the initial amount of radioactivity in liver tissue of mice receiving ^{89}Zr-**DFO**, ^{89}Zr-**1** or ^{89}Zr-**2** decreased by 72%, 49%, and 29%, respectively. Animals injected with ^{89}Zr-**DFO** had the least radioactivity in liver tissue by the end of this study, while liver tissue of animals injected with ^{89}Zr-**2** had roughly 6 fold more activity than in mice receiving ^{89}Zr-**1**. (^{89}Zr-**DFO** vs. ^{89}Zr-**1** vs. ^{89}Zr-**2**: (mean%ID/g±SD; [one-way ANOVA value]: 0.066±0.009 vs. 0.26±0.019 vs. 1.43±0.15; [F(2,15) = 445.0, p < 0.0001]). Since **2** is a more flexible structure compared to ligand **1**, ^{89}Zr in complex with **2** most likely undergoes facile transchelation within the liver. Considering that radioactivity was not cleared during this experiment, we surmise that the ^{89}Zr formed an insoluble precipitate within the liver tissue, and is most likely ^{89}Zr[Zr]-phosphate, which has been shown to be retained there without excretion [11].

Animals receiving ^{89}Zr-**DFO** had significantly less radioactivity in kidney tissue when compared to the ^{89}Zr-IAM complexes at every time point. By 72 h p.i., animals receiving ^{89}Zr-**DFO**, ^{89}Zr-**1** or ^{89}Zr-**2** had excreted 49%, 71%, and 54% of the activity recorded at 2 h (^{89}Zr-**DFO** vs ^{89}Zr-**1** vs. ^{89}Zr-**2**: (mean%ID/g±SD; [one-way ANOVA value]: 0.69±0.098 vs. 4.71 ±0.84 vs. 3.60±0.79; [F(2,15) = 82.11, p < 0.0001]). As the ^{89}Zr-IAM complexes diffuse from the blood pool into the kidney, pH may decrease, which can cause changes in the charge or structure of these radiometal complexes. These changes may induce aggregation or transchelation, which contribute to the retention of radioactivity in kidneys. Initially, less radioactivity was observed in the kidneys of mice injected with ^{89}Zr-**2**; however, the amounts for both IAM complexes become similar within 48 hours, consistent with the slower plasma clearance of ^{89}Zr-**2**. Further study is needed to ascertain whether increased radioactivity in the kidney relative to **DFO** would occur using antibody-chelator conjugates.

Since bone marrow is often considered a dose-limiting organ, radioactivity retention in bone was also examined [11]. Animals injected with either ^{89}Zr-IAM complex demonstrated significantly more radioactivity in their bone tissue when compared to animals injected with ^{89}Zr-**DFO** at 72 h p.i. (^{89}Zr-**DFO** vs ^{89}Zr-**1** vs. ^{89}Zr-**2**: (mean%ID/g±SD; [one-way ANOVA value]: 0.079±0.014 vs. 0.11±0.006 vs. 0.68±0.33; [F(2,15) = 17.57, p = 0.0001]). Interestingly, the biodistribution trends for ^{89}Zr-**1** and ^{89}Zr-**2** are very different. The amount of radioactivity in the bone of animals that received ^{89}Zr-**1** diminished over time, and may reflect perfusion and clearance kinetics rather than demetallation and incorporation into the bone matrix. A similar phenomenon has been observed with a recently described hydroxypyridinone ligand [14]. By contrast, radioactivity in the bones of mice receiving ^{89}Zr-**2** continually increased during this experiment, and most likely reflects radiometal chelate instability, transchelation, and metabolic sequestration of the ^{89}Zr within the phosphate-rich bone matrix.

Conclusions

Herein, we describe the synthesis and evaluation of hydroxyisophthalamide ligands as bifunctional chelators for ^{89}Zr using log P, DTPA, and serum challenge studies. Additionally, the biodistribution of ^{89}Zr-**1** and ^{89}Zr-**2** was evaluated in normal mice. While the preparation of ^{89}Zr-**1** required higher temperatures and longer reaction times compared to ^{89}Zr-**2**, it was more

resistant to exogenous ligand challenge. Animals injected with ^{89}Zr-**1** retained less radioactivity in the blood, liver, and bone than those receiving ^{89}Zr-**2**. These differences are believed to be caused by increased flexibility engineered into ligand **2**. These data suggest that IAM ligands, which were previously found useful for the sequestration of a variety of lanthanide metal cations, can also function as ^{89}Zr chelators. Additional ligands that synergize the facile radiochemistry of **2** with the enhanced stability demonstrated by ^{89}Zr-**1** are currently being evaluated in ^{89}Zr-immuno-PET applications, and will be reported in due course.

Supporting information

S1 Scheme. Synthesis of Zr-1.
(PDF)

S2 Scheme. Synthesis of Zr-2.
(PDF)

S1 Fig. ESI-MS analysis of Zr-1.
(PDF)

S2 Fig. ESI-MS analysis of Zr-2.
(PDF)

S3 Fig. Energy minimized structures of Zr-1 and Zr-2.
(PDF)

S4 Fig. Radio-ITLC analysis of ^{89}Zr(Ox)$_2$ (A), ^{89}Zr-1 (B) and ^{89}Zr-2 (C) using 50mM DTPA (pH 7) as eluent.
(PDF)

S5 Fig. Radio-HPLC of ^{89}Zr-1.
(PDF)

S6 Fig. Radio-HPLC of ^{89}Zr-2.
(PDF)

S1 Table. DFT coordinates for the energy minimized structures of Zr-1 and Zr-2.
(PDF)

S2 Table. Log P values for ^{89}Zr-complexes.
(PDF)

S3 Table. Stability of ^{89}Zr-complexes in 50 mM DTPA (pH 7).
(PDF)

S4 Table. Stability (% intact) of ^{89}Zr-complexes in human serum at 37˚C.
(PDF)

S5 Table. Biodistribution data of ^{89}Zr-1 in normal mice.
(PDF)

S6 Table. Biodistribution data of ^{89}Zr-2 in normal mice.
(PDF)

S7 Table. Biodistribution data of ^{89}Zr-DFO in normal mice.
(PDF)

Acknowledgments

Author Contributions

Conceptualization: NBB DNP JX DM TJW.

Data curation: NBB DNP JX DT DM TJW.

Formal analysis: NBB DNP JX DT DM TJW.

Funding acquisition: DM TJW.

Investigation: NBB DNP JX DT DM TJW.

Methodology: NBB DNP JX DT DM TJW.

Project administration: DM TJW.

Resources: DM TJW.

Supervision: DM TJW.

Validation: NBB DNP JX DT DM TJW.

Visualization: NBB DNP JX DT DM TJW.

Writing – original draft: NBB DNP JX DT DM TJW.

Writing – review & editing: NBB DNP JX DT DM TJW.

References

1. Mustafa MG, West HI Jr., O'Brien H, Lanier RG, Benhamou M, Tamura T. Measurements and a direct-reaction-plus-Hauser-Feshbach analysis of 89Y(p,n)89Zr, 89Y(p,2n)88, and 89Y(p,pn)88Y reactions up to 40 MeV. Phys Rev C Nucl Phys. 1988; 38: 1624–37. PMID: 9954974

2. Meijs WE, Herscheid JD, Haisma HJ. Production of highly pure no-carrier-added zirconium-89 for the labelling of antibodies with a positron emitter. Applied Radiation Isotopes. 1994; 45: 1143–7.

3. Verel I, Visser GW, Boellaard R, Stigter-van Walsum M, Snow GB, van Dongen GA. 89Zr immuno-PET: comprehensive procedures for the production of 89Zr-labeled monoclonal antibodies. J Nucl Med. 2003; 44: 1271–81. PMID: 12902418

4. Wadas TJ, Wong EH, Weisman GR, Anderson CJ. Coordinating radiometals of copper, gallium, indium, yttrium, and zirconium for PET and SPECT imaging of disease. Chem Rev. 2010; 110: 2858–902. https://doi.org/10.1021/cr900325h PMID: 20415480

5. Price EW, Orvig C. Matching chelators to radiometals for radiopharmaceuticals. Chem Soc Rev. 2014; 43: 260–90. https://doi.org/10.1039/c3cs60304k PMID: 24173525

6. Health NIo. Clinicaltrials.gov. Accessed May 02, 2017; Key words: Zirconium and PET.

7. Liu ZD, Kayyali R, Hider RC, Porter JB, Theobald AE. Design, synthesis, and evaluation of novel 2-substituted 3-hydroxypyridin-4-ones: structure-activity investigation of metalloenzyme inhibition by iron chelators. J Med Chem. 2002; 45: 631–9. PMID: 11806714

8. Liu ZD, Hider RC. Design of clinically useful iron(III)-selective chelators. Med Res Rev. 2002; 22: 26–64. PMID: 11746175

9. Holland JP, Divilov V, Bander NH, Smith-Jones PM, Larson SM, Lewis JS. 89Zr-DFO-J591 for immuno-PET of prostate-specific membrane antigen expression in vivo. J Nucl Med. 2010; 51: 1293–300. https://doi.org/10.2967/jnumed.110.076174 PMID: 20660376

10. Perez-Medina C, Abdel-Atti D, Zhang Y, Longo VA, Irwin CP, Binderup T, et al. A modular labeling strategy for in vivo PET and near-infrared fluorescence imaging of nanoparticle tumor targeting. J Nucl Med. 2014; 55: 1706–11. https://doi.org/10.2967/jnumed.114.141861 PMID: 25060196

11. Abou DS, Ku T, Smith-Jones PM. In vivo biodistribution and accumulation of 89Zr in mice. Nucl Med Biol. 2011; 38: 675–81. https://doi.org/10.1016/j.nucmedbio.2010.12.011 PMID: 21718943

12. Holland JP, Vasdev N. Charting the mechanism and reactivity of zirconium oxalate with hydroxamate ligands using density functional theory: implications in new chelate design. Dalton Trans. 2014; 43: 9872–84. https://doi.org/10.1039/c4dt00733f PMID: 24722728

13. Boros E, Holland JP, Kenton N, Rotile N, Caravan P. Macrocycle-Based Hydroxamate Ligands for Complexation and Immunoconjugation of 89Zirconium for Positron Emission Tomography (PET) Imaging. Chempluschem. 2016; 81: 274–81. https://doi.org/10.1002/cplu.201600003 PMID: 27630807

14. Deri MA, Ponnala S, Zeglis BM, Pohl G, Dannenberg JJ, Lewis JS, et al. Alternative chelator for (8)(9)Zr radiopharmaceuticals: radiolabeling and evaluation of 3,4,3-(LI-1,2-HOPO). J Med Chem. 2014; 57: 4849–60. https://doi.org/10.1021/jm500389b PMID: 24814511

15. Guerard F, Lee YS, Tripier R, Szajek LP, Deschamps JR, Brechbiel MW. Investigation of Zr(IV) and 89Zr(IV) complexation with hydroxamates: progress towards designing a better chelator than desferrioxamine B for immuno-PET imaging. Chem Commun (Camb). 2013; 49: 1002–4.

16. Guerard F, Lee Y-S, Brechbiel MW. Rational Design, Synthesis, and Evaluation of Tetrahydroxamic Acid Chelators for Stable Complexation of Zirconium(IV). Chem—Eur J. 2014; 20: 5584–91. https://doi.org/10.1002/chem.201304115 PMID: 24740517

17. Jacobson O, Zhu L, Niu G, Weiss ID, Szajek LP, Ma Y, et al. MicroPET imaging of integrin alphavbeta3 expressing tumors using 89Zr-RGD peptides. Mol Imaging Biol. 2011; 13: 1224–33. https://doi.org/10.1007/s11307-010-0458-y PMID: 21161690

18. Ma MT, Meszaros LK, Paterson BM, Berry DJ, Cooper MS, Ma Y, et al. Tripodal tris(hydroxypyridinone) ligands for immunoconjugate PET imaging with 89Zr4+: comparison with desferrioxamine-B. Dalton Trans. 2015; 44: 4884–900. https://doi.org/10.1039/c4dt02978j PMID: 25351250

19. Pandya DN, Pailloux S, Tatum D, Magda D, Wadas TJ. Di-macrocyclic terephthalamide ligands as chelators for the PET radionuclide zirconium-89. Chem Commun (Camb), 2015; 51: 2301–3.

20. Patra M, Bauman A, Mari C, Fischer CA, Blacque O, Haussinger D, et al. An octadentate bifunctional chelating agent for the development of stable zirconium-89 based molecular imaging probes. Chem Commun (Cambridge, U K). 2014; 50: 11523–5.

21. Price EW, Zeglis BM, Lewis JS, Adam MJ, Orvig C. H6phospa-trastuzumab: bifunctional methylene-phosphonate-based chelator with 89Zr, 111In and 177Lu. Dalton Trans. 2014; 43: 119–31. https://doi.org/10.1039/c3dt51940f PMID: 24104523

22. Rudd SE, Roselt P, Cullinane C, Hicks RJ, Donnelly PS. A desferrioxamine B squaramide ester for the incorporation of zirconium-89 into antibodies. Chem Commun (Cambridge, U K). 2016; 52: 11889–92.

23. Tinianow JN, Pandya DN, Pailloux SL, Ogasawara A, Vanderbilt AN, Gill HS, et al. Evaluation of a 3-hydroxypyridin-2-one (2,3-HOPO) based macrocyclic chelator for 89Zr4+ and its use for immunoPET imaging of HER2 positive model of ovarian carcinoma in mice. Theranostics. 2016; 6: 511–21. https://doi.org/10.7150/thno.14261 PMID: 26941844

24. Pandya DN, Bhatt N, Yuan H, Day CS, Ehrmann BM, Wright M, et al. Zirconium tetraazamacrocycle complexes display extraordinary stability and provide a new strategy for zirconium-89-based radiopharmaceutical development. Chem Sci. 2017; 8: 2309–14. https://doi.org/10.1039/c6sc04128k PMID: 28451334

25. Daumann LJ, Werther P, Ziegler MJ, Raymond KN. Siderophore inspired tetra- and octadentate antenna ligands for luminescent Eu(III) and Tb(III) complexes. J Inorg Biochem. 2016; 162: 263–73. https://doi.org/10.1016/j.jinorgbio.2016.01.006 PMID: 26832605

26. Law GL, Andolina CM, Xu J, Luu V, Rutkowski PX, Muller G, et al. Circularly polarized luminescence of curium: a new characterization of the 5f actinide complexes. J Am Chem Soc. 2012; 134: 15545–9. https://doi.org/10.1021/ja306354n PMID: 22920726

27. Xu J, Corneillie TM, Moore EG, Law GL, Butlin NG, Raymond KN. Octadentate cages of Tb(III) 2-hydroxyisophthalamides: a new standard for luminescent lanthanide labels. J Am Chem Soc. 2011; 133: 19900–10. https://doi.org/10.1021/ja2079898 PMID: 22010878

28. Samuel AP, Lunkley JL, Muller G, Raymond KN. Strong Circularly Polarized Luminescence from Highly Emissive Terbium Complexes in Aqueous Solution. Eur J Inorg Chem. 2010: 3343–7. https://doi.org/10.1002/ejic.201000309 PMID: 20730030

29. Seitz M, Do K, Ingram AJ, Moore EG, Muller G, Raymond KN. Circularly polarized luminescence in enantiopure europium and terbium complexes with modular, all-oxygen donor ligands. Inorg Chem. 2009; 48: 8469–79. https://doi.org/10.1021/ic901079s PMID: 19639983

30. Moore EG, Samuel AP, Raymond KN. From antenna to assay: lessons learned in lanthanide luminescence. Acc Chem Res, 2009; 42: 542–52. https://doi.org/10.1021/ar800211j PMID: 19323456

31. Samuel AP, Xu J, Raymond KN. Predicting efficient antenna ligands for Tb(III) emission. Inorg Chem. 2009; 48: 687–98. https://doi.org/10.1021/ic801904s PMID: 19138147

32. Samuel AP, Moore EG, Melchior M, Xu J, Raymond KN. Water-soluble 2-hydroxyisophthalamides for sensitization of lanthanide luminescence. Inorg Chem. 2008; 47: 7535–44. https://doi.org/10.1021/ic800328g PMID: 18671388

33. Cohen SM, Petoud S, Raymond KN. A Novel Salicylate-Based Macrobicycle with a "Split Personality". Inorg Chem. 1999; 38: 4522–9. PMID: 11671166

34. Frisch M, Trucks G, Schlegel H, Scuseria G, Robb M, Cheeseman J, et al. Gaussian 09 D.01 ed. Wallingford, CT: Gaussian, Inc. 2009.

35. Hehre W, Ditchfield R, Pople J. Self—Consistent Molecular Orbital Methods. XII. Further Extensions of Gaussian—Type Basis Sets for Use in Molecular Orbital Studies of Organic Molecules. Journal of Chemical Physics. 1972; 56: 2257–67.

36. Hariharan P, Pople J. The influence of polarization functions on molecular orbital hydrogenation energies. Theroretical Cehmical Accounts. 1973; 28: 213–22.

37. Francl M, Pietro W, Hehre W, Binkley J, DeFrees D, Pople J, et al. Self-consistent molecular orbital methods. XXIII. A polarization-type basis set for second-row elements. Journal of Chemical Physics. 1982; 77: 3654–65.

38. Petersson G, Bennett A, Tensfeldt T, Al-Laham M, Shirley W, Mantzaris J. A complete basis set model chemistry. I. The total energies of closed-shell atoms and hydrides of the first-row elements Journal of Chemical Physics. 1988; 89: 2193–218.

39. Andrae D, Haeussermann U, Dolg M, Stoll H, Preuss H. Energy-adjustedab initio pseudopotentials for the second and third row transition elements. Theoretical Chimica ACta. 1990; 77: 123–41.

40. Martin J, Sundermann A. Correlation consistent valence basis sets for use with the Stuttgart–Dresden–Bonn relativistic effective core potentials: The atoms Ga–Kr and In–Xe. Journal of Chemical Physics. 2001; 114: 3408–20.

41. Waterhouse RN. Determination of lipophilicity and its use as a predictor of blood-brain barrier penetration of molecular imaging agents. Mol Imaging Biol. 2003; 5: 376–89. PMID: 14667492

42. Wadas TJ, Sherman CD, Miner JH, Duncan JR, Anderson CJ. The biodistribution of [153Gd]Gd-labeled magnetic resonance contrast agents in a transgenic mouse model of renal failure differs greatly from control mice. Magn Reson Med. 2010; 64: 1274–80. https://doi.org/10.1002/mrm.22553 PMID: 20648683